Experimental reconstruction of extreme sea waves by time reversal principle

Guillaume Ducrozet, Félicien Bonnefoy, Nobuhito Mori, Mathias Fink, Amin Chabchoub

Experimental reconstruction of extreme sea waves by time reversal principle

Guillaume Ducrozet[1] †, Félicien Bonnefoy[1], Nobuhito Mori[2], Mathias Fink[3] and Amin Chabchoub[4]

[1]École Centrale de Nantes, LHEEA Res. Dept. (ECN and CNRS), 1 rue de la Noé - 44321 Nantes, France

[2]Disaster Prevention Research Institute, Kyoto University, Kyoto 611-0011, Japan

[3]Institut Langevin, ESPCI Paris, PSL University, CNRS, UMR CNRS No. 7587, 10 rue Vauquelin, 75005 Paris, France

[4]Centre for Wind, Waves and Water, School of Civil Engineering, The University of Sydney, Sydney, NSW 2006, Australia

(Received xx; revised xx; accepted xx)

We report an experimental study on the reconstruction of real-ocean rogue waves in a laboratory environment using the time reversal (TR) methodology (Chabchoub & Fink 2014). Three different rogue wave measurements are used to validate the TR approach. The generation and accurate control of target free surface profiles in a unidirectional wave flume using standard techniques, such as the New Wave Theory (Tromans *et al.* 1991) is fairly challenging, especially, for very steep and thus, highly nonlinear extreme waves. The TR method, making use of the time reversibility of the wave propagation and symmetry of the governing hydrodynamic equations of motion, leads to a simple two-step experimental procedure, which accuracy is investigated in this paper. The use of the TR procedure requires the appropriate Froude scaling in designing the model-scale experiments. The present study represents the first validation of the TR method to realistic irregular seas containing rogue waves. The three extreme wave profiles are tested to assess the applicability of the TR scheme on different wave configurations taking into account variable characteristics. This includes the famed New Year wave. The accuracy of the TR method is demonstrated with varying wave steepness values and propagation distances of the reverse reconstruction. It is demonstrated that the unidirectional TR reconstruction is robust, even in the presence of unavoidable wave breaking, known to be an irreversible process within the framework of any wave hydrodynamic evolution equation, and independently of complex environmental conditions or focusing mechanism at play in the sea.

1. Introduction

The application of the elegant Time Reversal (TR) principle (Fink 1992) in the context of water waves to refocus nonlinear and extreme waves in a hydrodynamic wave flume has been recently studied experimentally and numerically (Chabchoub & Fink 2014; Ducrozet *et al.* 2016*b*). Those studies take as reference wave profiles from exact analytic solutions of the nonlinear Schrödinger equation (NLSE) (Zakharov 1968). Assuming time reversibility of the process, the concept consists in firstly generating a wave group at its maximal compression state and then measuring its attenuated profile at a well-defined mirror position. Using the symmetry of the latter evolution equation allows the

† Email address for correspondence: guillaume.ducrozet@ec-nantes.fr

interchangeability of the mirror and source location. As such, the backwards generation of the time-reversed attenuated wave profile from the mirror, that is expected to refocus at the wave maker source location, is equivalent to the generation of the same time-reversed attenuated wave profile at the wave maker and expecting the refocusing at the mirror location. Earlier experiments (Baldock *et al.* 1996) have shown that the wave profile measured after a large focused wave group is identical to the time-reversed profile of the wave field at the opposite location before the focused wave. The comprehensive numerical study provided in (Ducrozet *et al.* 2016*b*) assessed the applicability of the TR refocusing procedure over a wide range of propagating distances and initial wave steepness for different analytic solutions of the NLSE (stationary envelope soliton and doubly-localized Peregrine-type breathers of first and second-order (Peregrine 1983; Akhmediev *et al.* 1985)), thus, over a wide range of dispersion and nonlinearity parameters. When dealing with pulsating solutions exhibiting large amplifications of the carrier wave, as the case for breathers (Onorato *et al.* 2013; Dudley *et al.* 2014; Chabchoub *et al.* 2016), it can be implied that the TR procedure, applied experimentally to the properly scaled real-ocean rogue waves in a water wave flume, will provide an accurate refocusing up to limiting thresholds, such as the characteristic steepness of the considered wave field.

The dependence of the practicality of the TR procedure for water waves in a wave tank configuration relies on some assumptions resulting in the violation of time-reversibility, on the other hand its range of applicability, dependent of propagating distance and degree of nonlinearity, is still quite remarkable. As consequence, it appears to be tempting to test its validity in the reproduction of measured ocean extreme waves in a laboratory environment. The reconstruction of rogue waves using the dispersive focusing mechanism, also known as New Wave Theory, has been demonstrated to be fairly challenging in practice (Tromans *et al.* 1991; Chaplin 1996; Clauss & Schmittner 2007; Schmittner *et al.* 2009; Fernandez *et al.* 2014; Ducrozet *et al.* 2016*a*; Alberello *et al.* 2018) and any development of a simple and efficient procedure is of major significance for the nonlinear and experimental water wave physics as well as ocean engineering communities.

The present study provides the first validation of the TR procedure on real-ocean rogue waves, measured in different geographic locations. Previous works dealing with the experimental application of the TR method to water waves were so far limited to the use of reference waves from analytic solutions of the NLSE (Chabchoub & Fink 2014; Ducrozet *et al.* 2016*b*). These are valid only for unidirectional, weakly nonlinear and narrow-banded wave fields. The extreme waves at sea are known to be more complex (highly non-linear, broad frequency content and with possible directional spreading) (Kharif *et al.* 2009). The latter limitations are overcome with the present choice of extreme wave profiles measured at sea. The objective of this paper is consequently to assess the accuracy of the TR procedure for reproducing these real-ocean rogue waves in water wave facilities. The series of laboratory experiments have been conducted in the deep large towing tank of École Centrale Nantes (ECN). It is shown that these extreme waves can be perfectly reconstructed at a reasonable distance from the wave maker for all scales and nonlinearity range.

We focus on the reproduction in a unidirectional tank of the three measured extreme wave profiles. Consequently, the directionality of the underlying sea state is not taken into account, whereas obviously present in a real wave field. This is an important feature in the formation of extreme events, especially when it comes to the understanding of the physics of their appearance (the role of modulational instability, the effect of directional focusing, etc.), see (Onorato *et al.* 2009; Mori *et al.* 2011; Fedele *et al.* 2016; Fujimoto *et al.* 2019). However, the simplified unidirectional wave propagation as such is still

relevant for state of the art water wave facilities with single wave maker and there is a need for accurate and effective extreme wave reproduction procedures.

The paper is structured as the follows. Section 2 will introduce the methodology employed as well as the experimental set-up. Subsequently, Section 3 reports the results of the laboratory experiments followed by a conclusive Section 4.

2. Methodology and experimental set-up

In this section, we will recall the main results of previous studies (Chabchoub & Fink 2014; Ducrozet *et al.* 2016*b*) that have demonstrated the possibility of the use of TR mirror to refocus extreme water waves obtained from analytic solutions to NLSE in a water wave facility. The TR procedure is briefly explained, followed by a description of the different rogue wave profiles used in the study. Ultimately, the experimental set-up is presented.

2.1. *Time-Reversal wave refocusing procedure*

Time-reversal mirrors are widely used to refocus acoustic signals (Fink 1999). The methodology has been proven to be very useful in other physical media, such as optics (Carminati *et al.* 2007) and water waves (Fouque & Nachbin 2003). The concept intrinsically uses the time-reversal symmetry of wave propagation that exists in the absence of dissipation (in a conservative medium) to reconstruct the past evolution of wave dynamics. Consequently, this concept can be used to refocus extreme wave localisations. As shown next, the symmetry of the hydrodynamic evolution framework appears to be a useful feature to translate the extreme wave from the location of generation to any position in a water wave facility. Therefore, this experimental two-step concept is very powerful for ocean engineering applications as two experiments only are required to reconstruct any extreme wave event at an arbitrary position of interest in a laboratory environment.

2.1.1. *Practical application in water wave tanks*

Hydrodynamic experiments using the two-step TR focusing have been reported in (Przadka *et al.* 2012) for linear waves and further extended to nonlinear localised wave profiles in (Chabchoub & Fink 2014). Earlier, time-reversal characteristics have already been detected in (Baldock *et al.* 1996; Shemer *et al.* 2007). The TR refocusing procedure is generally initiated by a well-defined wave profile / pulse of interest $\eta_T(t)$ at the source position x_S as a first step. This pulse will then propagate in space and time while wave profiles can be measured at different locations along the facility, which correspond to mirror locations x_M (in a wave hydrodynamic experiment this corresponds to the locations of the wave gauges). At x_M the signal is then time-reversed and sent back to the source location x_S. If characteristic TR features are not violated, the waves will refocus at x_S, independently of the complexity of the medium. In (Chabchoub & Fink 2014) it has been shown that the symmetry of the NLSE can be used to re-inject the time-reversed signal at the source position x_S (rather than re-emitted in x_M) as a second experimental step and expect refocusing at the mirror x_M (instead of x_S). Each of the mirror locations can correspond to an arbitrary wave gauge location. As will be shown, this methodology appears to be very useful to reconstruct extreme waves at any desired position in the flume in a straightforward way.

For practical applications, one has to define the time window used during the first propagation $T_{\mathrm{win_{FP}}}$, which is usually short and centred around the extreme wave of

interest. The wave gauge measurement at the mirror location x_M is also time windowed before its use as input time-reversed signal. For this purpose, we ensure that the slower waves, defined by the maximum frequency $f_{\max}$, are recorded within this TR time window $T_{\mathrm{win_{TR}}}$. It is then defined to be

$$T_{\mathrm{win_{TR}}} = T_{\mathrm{win_{FP}}} + x_M/C_g(f_{\max}), \tag{2.1}$$

while C_g denotes the linear group velocity of wave packets in deep-water defined to be $C_g(f) = \pi f/k$, f and k are the frequency and wave number, respectively.

2.1.2. *Wave reflections from the absorbing beach*

In a water tank facility, the wall opposite to the wave generation system is usually equipped with an absorbing beach, designed to reduce the amount of reflected waves. We assume that our signal is composed of waves at different frequencies and we aim to evaluate the spatial extent of the region that is free of those beach-reflected waves. This is of particular importance in experiments for which the wave absorption is never assumed to be optimal.

To quantify this, we determine the maximum wave frequency of the signal $f_{\max}$ (slower waves) as well as the minimum frequency $f_{\min}$ (faster waves). These definitions rely on a level of energy that is assumed as acceptable, i.e. sufficiently small to not induce any inaccuracies in the procedure.

The waves are generated during a given time window T_{win} and the wave tank has a specific length L_x. At the time of reflection, the wave front of slower waves has reached a distance of x_r and the faster waves a distance of $2L_x - x_r$. These distances can be connected and evaluated using the following relationship

$$T_{\mathrm{win}} + x_r/C_g(f_{\max}) = (2L_x - x_r)/C_g(f_{\min}), \tag{2.2}$$

For a given wave field and as such a spectral distribution with fixed values of $f_{\max}$ and $f_{\min}$ that is generated for a given duration T_{win}, the spatial extent free of reflections is consequently dependent on the size of the wave tank L_x. Obviously, a longer tank allows a longer reflection-free spatial zone.

In other words, dependent on the choice of the time window and location of the mirror location x_M, it is clear that the amount of possible reflected waves from the beach will be different. Consequently, for a given range of frequencies, the longer the propagating distance, the shorter the time window being free of reflections. Note that the wave frequencies are usually chosen so that the absorbing beach is efficient and performs a low reflection rate. Typically, the amount of reflected wave amplitudes corresponding to large frequencies is lower than $5-10\%$. However, this rate may be far larger when dealing with low frequencies in a wave spectrum, up to $20-30\%$ in the present study.

2.1.3. *Wave generation*

As previously described, the TR procedure relies on the definition of an adequate wave maker motion from a free surface profile. At first, we define time-series ramps at the beginning and end of the chosen time window in order to ensure (i) a smooth initialisation of the wave maker's movement and (ii) the periodicity of the signal, which is decomposed on Fourier components. Then, the effective motion is defined using a linear transfer function to initiate the wave profiles (Chabchoub & Fink 2014; Ducrozet *et al.* 2016*b*). This latter linearization has been identified as a possible source of inaccuracy in the TR procedure. Hence, enhancements of the wave generation process have been performed in the current study. Notoriously, during the wave generation process by a wave maker, the so-called evanescent waves are spontaneously created when the wave

field is generated. These waves are only relevant close to the wave generator since they rapidly decay after a very short propagation distance (Dean & Dalrymple 1991). In the large configuration tested, they are therefore negligible considering the whole range of propagation distances for $kx_M \geqslant 15$. In addition, parasitic second-order free waves are also generated with the target wave field (Schäffer 1996). These waves are expected to be at the origin of the reduced accuracy at relative small propagating distances described in (Ducrozet *et al.* 2016*b*). Indeed, within this range of propagation distance, the parasitic free waves are recorded after the first propagation. Consequently, during the refocusing of the waves, the latter are generated again and indeed interfere with the localised structure, reducing the corresponding accuracy. A specific procedure has been set-up to control the generation of those parasitic waves produced by the wave maker (Schäffer 1996).

A second source of disturbance is associated to the use of a free surface measurement to initiate the TR procedure. These measurements include by nature all the nonlinearities of the wave field. That is, a linear transfer function is directly used to determine the wave maker's motion, the nonlinear components (and especially the bound contributions) are treated as linear free waves. In the context of a reference wave profile defined by analytic solutions of the NLSE (Chabchoub & Fink 2014; Ducrozet *et al.* 2016*b*), it is in fact straightforward to obtain the linear free waves components only. However, when using a measurement at sea this appears far more complicated. As such, it is not possible from a single-point broad-banded measurement to distinguish between bound and free waves. When dealing with an extreme wave that exhibits a high degree of nonlinearity this may indeed induce significant differences. This issue can be partly addressed by removing the second-order components of the considered wave field. This procedure assumes the original free-surface measurement as a linear wave field and deduces the corresponding second-order components (Dalzell 1999). These are then removed from the original measurement to deduce a new set of linear components. An iterative process is applied to analyse the convergence of the sum of the linear and the second-order components toward the original measurements at sea.

2.2. *Three different extreme wave profiles*

During this study, the reproduction of three different rogue wave profiles will be investigated. The first one is the well-known New Year wave recorded on January 1st, 1995 at the Draupner platform in the North Sea (Haver 2004). This is the first scientific measurement of a rogue wave and as such, has been widely studied as a reference event for extreme waves. This famed wave has been accurately reconstructed using the interference or dispersive focusing mechanism in a unidirectional wave flume (Clauss & Klein 2011) and more recently in a directional flume for crossing seas with a crossing angle of 120° (McAllister *et al.* 2019). The second and third wave profiles have been measured in the Sea of Japan at a location 3 km of the Yura fishery harbour (Liu & Mori 2001). The temporal free surface profiles for the three rogue waves chosen are given in figure 1 over a standard time window of 20 minutes.

Table 1 summarises the characteristic properties of the three different rogue wave profiles chosen in this study. The degree of nonlinearity is here characterized by the ratio $H_{\max}/H_s$ and $H_{\max}/\lambda_p$. $H_{\max}$ stands for the maximum wave height extracted from the temporal signal with zero up-and-down-crossing analyses, H_s is the significant wave height defined from the wave spectrum $S(f)$ as $H_s = H_{m_0} = 4\sqrt{m_0} = 4\sqrt{\int S(f)df}$ and λ_p is the peak wavelength defined from the peak period T_p of the spectrum and the linear dispersion relation $\omega = \sqrt{gk\tanh(kh)}$ with h standing for the water depth. $H_{\max}/H_s$

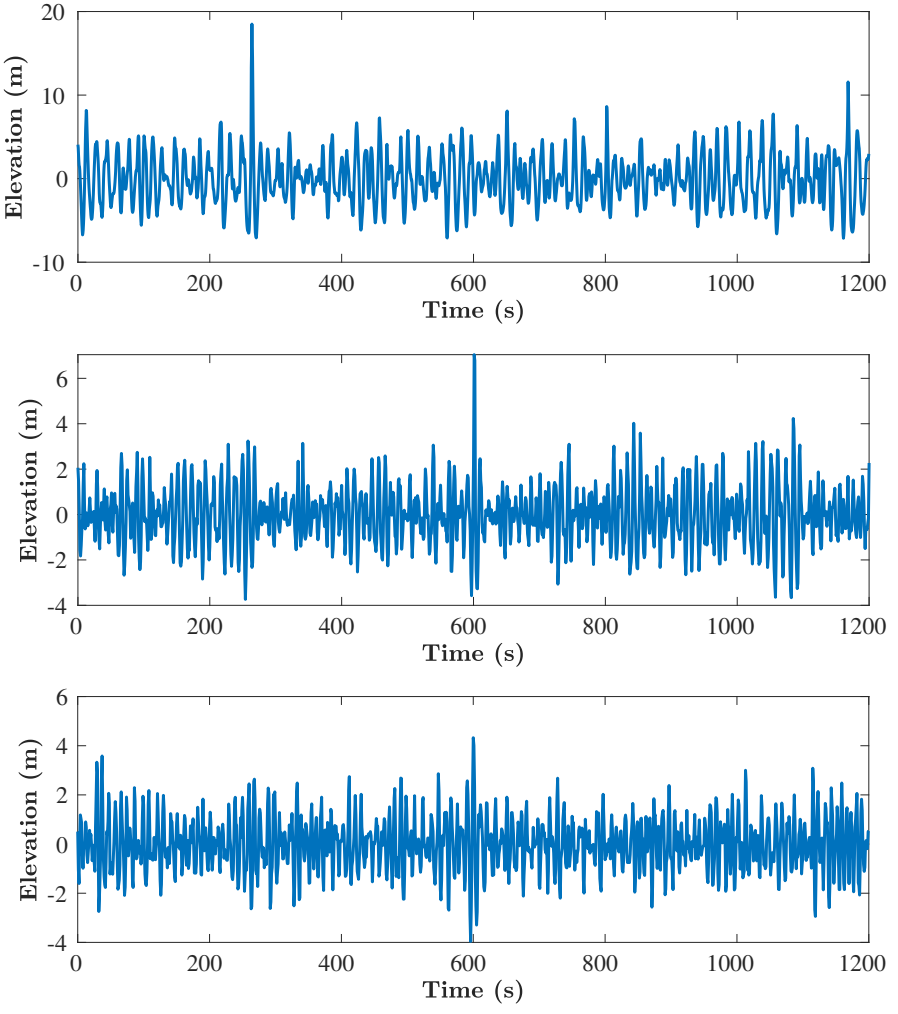

FIGURE 1. Full scale measured wave profiles. (Top) New Year wave. (Center) Yura wave 1. (Bottom) Yura wave 2.

describes the so-called abnormality index (Kharif *et al.* 2009) of the highest wave while $H_{\max}/\lambda_p$ is therefore also a measure of the degree of local nonlinearity of the extreme wave event, which should exceed twice the value of the characteristic wave steepness.

Based on these features, it is expected that the Yura waves exhibit a lower level of nonlinearity compared to the New Year wave. However, the wave referred to as Yura 1 is expected to have a lower probability of occurrence than the New Year wave, since it manifests a larger abnormality index. Those three waves are relatively steep and it is possible that wave breaking may have occurred for the extreme waves detected, even if the mean steepness of the wave fields $H_s/\lambda_p \in [0.030; 0.040]$ is not among the steepest possible sea-states, see e.g. measurements in North Sea (Haver *et al.* 2002; Ducrozet *et al.* 2017)). All three events appear in intermediate water depth, characterized by the relative water depth h/λ_p.

Those three wave profiles, which have been identified as rogue wave events, show different physical features that will enable to test the TR procedure in different contexts.

	New Year wave	Yura wave 1	Yura wave 2
Water depth - h (m)	70	43	43
Peak period - T_p (s)	14.4	10.4	9.59
Sig. wave height - H_s (m)	11.9	4.77	4.36
Mean steepness - H_s/λ_p	0.041	0.030	0.032
Rel. water depth - h/λ_p	0.24	0.27	0.31
$H_{\max}$ (m)	25.6	10.6	8.37
$H_{\max}/H_s$	2.15	2.23	1.92
$H_{\max}/\lambda_p$	0.087	0.067	0.061

TABLE 1. Characteristics of the three extreme wave recordings

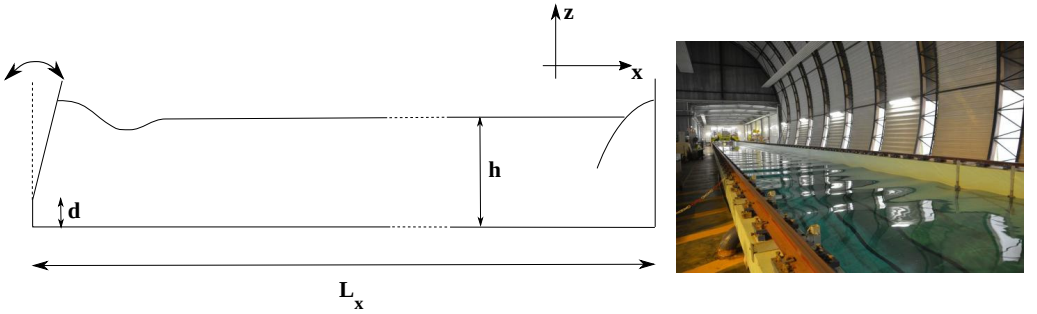

FIGURE 2. (Left) Sketch of the towing tank. (Right) Picture of the installation.

Note that the so-called Yura 2 wave is referenced as a rogue waves, even if the ratio $H_{\max}/H_s$ is less than the typical threshold of 2. As detailed in (Liu & Mori 2001), the identification of such extreme events can be achieved using the wavelet spectrum. In the case of rogue waves, strong energy density in the spectrum instantly appears and is carried over to the high frequency components, even at early stage of evolution (Cousins & Sapsis 2016).

2.3. *Experimental study in a water wave tank*

The present set of experiments is conducted in the large scale towing tank of ECN, which is $L_x = 140$ m long, 5 m wide and $h = 3$ m deep. Figure 2 provides a schematic view of the facility along with a picture. It is equipped with a flap-type wave maker on one side of the tank to generate unidirectional wave field in the range $f \in [0.15; 2]$ Hz. This wave maker is hinged at a distance $d = 0.15$ m from the bottom while its displacement can be accurately controlled. On the other side of the tank, an absorbing beach is installed to limit the wave reflections. The main advantage of the present wave tank is its length, which allows measurements free of any reflected waves considering a significant time windows, Eq. (2.2).

2.3.1. *Choice of the wave scales*

When performing experiments in a wave tank, the corresponding scale has to be chosen carefully regarding the Froude similarity at use in the present case of gravity waves. In addition, the possible limitations of the generation system, that consist of the maximum displacement of the paddle, its maximum velocity as well as the frequency range, have to be taken into account for an accurate wave generation. The latter constraints are partic-

	New Year wave	Yura wave 1	Yura wave 2
Scale	1/80	1/40	1/25
H_s (m)	0.15	0.12	0.17
f_p (Hz)	0.62	0.60	0.52
h/λ_p	0.74	0.69	0.52
Filt. ratio ($f_{\max} = 2$ Hz)	0.87	0.92	0.98

TABLE 2. Characteristics of the sea states at model scale

ularly important when dealing with highly nonlinear waves exhibiting broad frequency content. The wave generator in the towing tank facility can accurately generate waves from the frequency $f_{\min} = 0.15$Hz up to $f_{\max} = 2$ Hz. Regarding the latter limit, it is necessary to filter out the higher frequencies, which will not be generated correctly. This may induce significant discrepancies on the expected free surface elevation if the scale is not chosen correctly, i.e. if the scale is not adapted to the facility with significant energy content above $f_{\max}$.

Complementary, the geometry of the experimental facility has to be considered. It is indeed necessary to scale the water depth in order to have the exact same physics for the wave evolution between real and model scale. However, the flap-type wave maker prevents from changing the water depth in our experiments since a reduction induces a decrease of the largest wave possibly generated. Then, the wave field has to be scaled using the previously described wave maker capabilities, favouring the accuracy of the waves generated over the scaling of the water depth. The TR procedure is applied here to reproduce a temporal wave signal in a tank of arbitrary water depth.

As a consequence, the choice of the scale for the three locally focused reference wave profiles chosen is different as reported in table 2. In this table the significant wave height, the peak frequency f_p and the relative water depth at model scale together with a so-called filtering ratio is presented. Comparing with table 1, the model-scale configuration appears to be in a deep-water regime for the three reference extreme waves. This implies that the underlying physics of the full-scale and model-scale wave fields are different. Indeed, the change in relative water depth is expected to enhance the effect of modulational instability in the proposed experiments compared with the measurements at sea. However, it is anticipated that the assessment of the quality of the TR reproduction procedure in a tank of arbitrary water depth applies to a configuration in which correct Froude scaling is used.

The filtering ratio corresponds to the effect of the wave maker's limited accurate frequency range on the amplitude of the extreme wave generated. The original ocean rogue wave measurements at sea, as shown in figure 1, are filtered with a low-pass filter in the range $[0; f_{\max}]$. Then, the filtering ratio compares the amplitude of the filtered extreme wave with the amplitude of the original measurement.

2.3.2. *Experimental set-up*

A set of 17 wave gauges is installed along the wave tank in order to record the temporal evolution of the free surface elevation at different locations in the range of $x \in [15\,\text{m};\ 60\,\text{m}]$. The exact locations are provided in table 3. A sketch of the configuration with the locations of the probes is shown in figure 3.

We use resistance-type wave probes, which have been calibrated before the experimen-

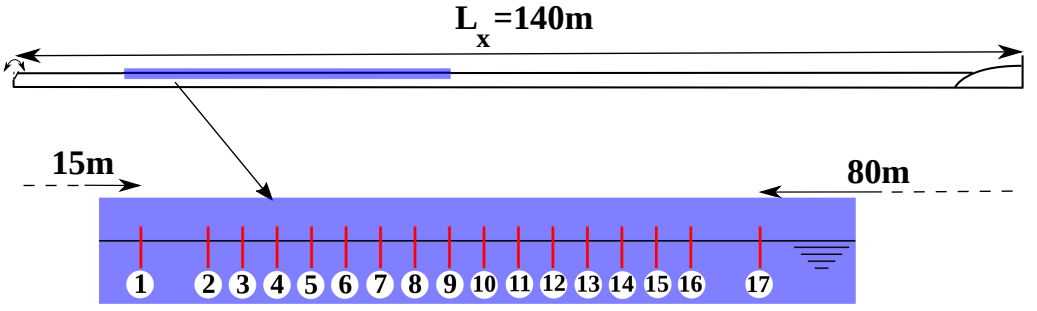

FIGURE 3. Sketch of the towing tank with the location of the probes

Probe No.	1	2	3	4	5	6	7	8	9	10	11	12	13	14	15	16	17
Location (m)	15	20	22.5	25	27.5	30	32.5	35	37.5	40	42.5	45	47.5	50	52.5	55	60

TABLE 3. Probe locations in the wave tank

tal campaign. These provide accurate free surface measurements at a sampling rate of 100 Hz. The data acquisition is triggered by the wave maker's motion start in order to ensure a correct synchronization of the measurements.

2.3.3. *Set of experiments*

As reported in (Ducrozet *et al.* 2016*b*), the TR method in deep water is influenced by the steepness of the wave field as well as the distance from the wave generator chosen for the mirror location x_M. This governed the choice of the set of tests presented in next Section. In view of covering the reproduction of a large range of wave profiles features, both, the amplitude of those waves and the mirror location are varied. As a summary, the following tests have been conducted:

- The three wave profiles described previously (Sec. 2.2) are considered, namely New Year, Yura 1 and Yura 2 waves.
- Different amplitude ratios are tested for each rogue wave profiles. This ratio is the scaling applied to the target free surface elevation, keeping the time-scale unchanged, in order to test the influence of the steepness on the quality of the wave reconstruction using TR.
- Three different probes are used as mirror locations x_M. These define the distance of the wave reconstruction from the wave maker. These probes are referred to by numbers 1, 6 and 16 in table 3. The corresponding distances are $x_M \in [15\,\mathrm{m};\ 30\,\mathrm{m};\ 55\,\mathrm{m}]$.

Tables 4 & 5 summarize the corresponding characteristics of the wave field in terms of local and mean steepness as well as the relative propagating distances at the three locations chosen.

3. Experimental results

In this section we report the experimental analysis related to the reconstructed ocean extreme sea states as in the North Sea and Sea of Japan using the TR approach. We first discuss the observations relative to the presence of breaking waves during the experiments. Then, we report an example of wave profiles, obtained during the first propagation before presenting the comprehensive results of the reconstruction procedure.

	Amp. ratio	Local steepness $H_{\max}/\lambda_p$	Mean steepness H_s/λ_p
New Year wave	30%	0.026	0.012
	60%	0.052	0.024
	85%	0.074	0.035
	100%	0.087	0.041
Yura wave 1	30%	0.020	0.0090
	60%	0.040	0.018
	85%	0.057	0.026
	100%	0.067	0.030
Yura wave 2	30%	0.018	0.0095
	60%	0.036	0.019
	85%	0.052	0.027
	100%	0.061	0.032

TABLE 4. Local and mean steepnesses as a function of the amplitude ratio for the three different wave profiles

	Probe No.	Non-dim. dist. $k_p x$
New Year wave	1	26
	6	51
	16	94
Yura wave 1	1	23
	6	47
	16	86
Yura wave 2	1	17
	6	34
	16	62

TABLE 5. Relative propagating distances as a function of the probe used for TR for the three wave profiles

3.1. *Experimental step 1: reference extreme wave generation*

The presence of breaking waves in the course of the experiments is crucial in the context of the TR method. This procedure indeed relies on the reversibility of the wave propagation process. This reversibility condition can be violated when wave breaking occurs. This phenomenon is known to induce wave energy dissipation through viscosity, mixing, etc., which are non-reversible effects (Babanin 2011).

It is then expected that the presence of wave breaking has a strong influence on the quality of the TR reconstruction. Table 6 provides a summary of the observations during the experiments with respect to the presence of wave breaking.

During the first propagation, it is expected that a rogue wave, which is highly localised in space and time, will defocus and disperse during its propagation when generated by the wave generator at x_S. The wave breaking probability is consequently expected to be

	Amp. ratio	Wave breaking during FP	Wave breaking during TR No. 1	No. 6	No. 16
New Year wave	30%	N	N	N	N
	60%	N	N	N	N
	85%	N	Y_2	N	N
	100%	Y_1	Y_3	Y_2	N
Yura wave 1	30%	N	N	N	N
	60%	N	N	N	N
	85%	N	N	Y_3	N
	100%	N	Y_2	Y_2	Y_2
Yura wave 2	30%	N	N	N	N
	60%	N	N	N	N
	85%	N	N	N	N
	100%	N	N	N	N

TABLE 6. Observations during experiments: First Propagation (FP) and TR. Y and N stand for (Yes) and (No) with respect to the presence of wave breaking in the course of the experiment. Index 1 indicates a wave breaking close to the wave generation system, 2 stands for wave breaking close to the wave probe and 3 denotes a wave breaking just after the wave probe.

larger close to the wave maker. It was observed that the New Year wave at maximum amplitude is the only configuration experiencing wave breaking, which indeed appears localised close to the wave maker.

Complementary, during the effective reproduction of the extreme wave profiles, refocusing will occur up to the mirror location x_M chosen for the TR approach. Wave breaking, if present, is expected to be located close to this probe during the TR reconstruction process. In the experiments conducted, both, New Year and Yura 1 waves are prone to the appearance of breaking waves, due to the significance of the local steepness of these waves see table 1). These events always appear at the focusing region and are limited, as expected, to the highest amplitude ratios 85% and 100%.

3.2. *Wave propagation tracking and wave reflection analysis*

During the first propagation of the wave field, the results are similar in terms of wave reflection analysis for the three wave profiles at use. We consequently limit the content of this section to the case of the New Year wave.

Figure 4 presents the temporal free surface profiles on the 17 wave gauges obtained for the 100% amplitude scaled New Year wave (i.e. the target rogue wave). For clarity, the different probes are vertically shifted with respect to their location in the water tank. In addition, this latter figure 4 includes different lines that depict the location of the wave fronts at the different probes locations. Those are useful to assess the possible presence of wave reflection during the measurements. Here, three different wave fronts are considered:

- $f_{\min}$ line depicts the propagation of the wave front associated to the lower frequency waves generated by the wave maker. This indicates the location of this wave front for each temporal probe signal. The second part of the line (vertically descending) represents this wave front after its reflection on the absorbing beach. This line is essential to analyse the presence of wave reflections in the experiments conducted.
- f_p line is the same than previous one, but for the peak frequency.
- $f_{\max}$ line represents the location of the wave front associated with the maximum

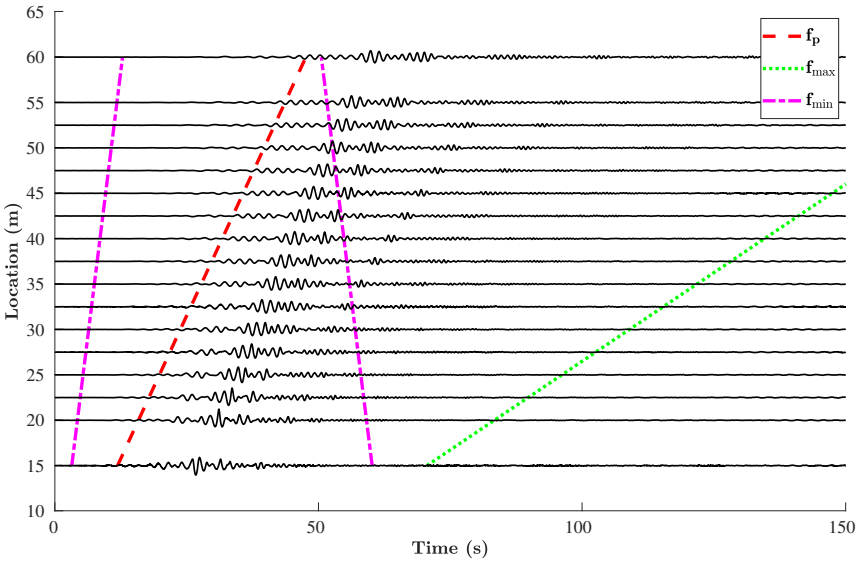

FIGURE 4. First propagation for New Year wave with 100% amplitude. Vertically shifted probes temporal signals (solid lines) together with wave fronts for different frequencies (see text for details)

frequency $f_{\max}$ generated by the wave maker. It starts at the end of the first propagation time window $T_{\mathrm{win_{FP}}}$ to depict the wave front of the end of the experiment (also referred as wave tail). This is the final time with relevant frequency content, which consequently defines the time window at use for the TR experiment (Eq. (2.1)).

The different probes temporal signals allow an overview of the space-time evolution of the considered wave sequence imposed at the wave maker location. We can clearly observe the attenuation of the initial rogue wave profile and especially the effect of the dispersion on the initial extreme event. On this relatively long propagation distance $k_p x_{\max} \simeq 100$, we notice that the initial localised free surface profiles evolve toward different wave packets that propagate with their own speeds.

While observing the different wave fronts, it is also interesting to indicate that it appears almost impossible to eliminate the reflection of the lower frequencies, even if their energy is assumed to be very small over the whole time window used for the refocusing experiment, see dotted green line $f_{\max}$.

On the other hand, if one considers the peak frequency as the relevant one, this ensures a quite large time window free of reflections. In a practical point of view, when considering wave probes further in the wave tank, the amount of reflected waves is assumed to become gradually larger. In this respect, the length of the water tank at use allows to delay the appearance of those reflected waves and consequently reduce their energy content.

As a reminder, the probes used to determine the mirror location for the TR are probes No. 1, 6 and 16. They can be consequently considered as free of reflection, with a limited amount of reflection and possibly influenced by reflection, respectively.

Figure 5 presents the effect of the nonlinearity during the first propagation of the wave field. The normalized free surface elevation is presented $\eta^* = \eta/\mathrm{Amp.}$ ratio at the three

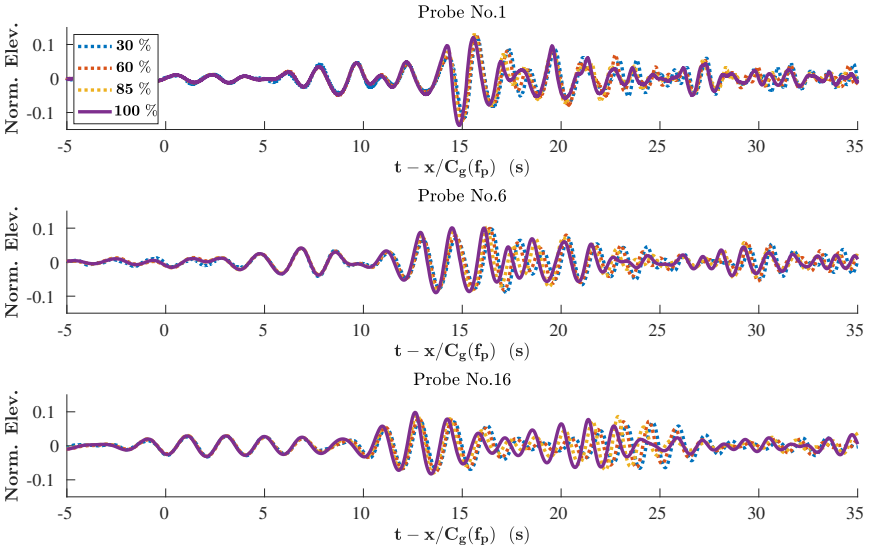

FIGURE 5. Effect of the nonlinearity during first propagation - New Year wave

probes No. 1, 6 and 16, which are used in the following for the TR procedure. The time is then shifted with the group velocity at the peak of the wave spectrum $C_g(f_p)$ for correct alignment of the wave groups.

The importance of the nonlinearities during the propagation in the wave tank is clearly demonstrated. Large discrepancies are observed when changing the amplitude ratio of the initial wave maker motion, especially, in terms of phase velocities of the different wave components. In fact, a significant phase shift is observed on probe No. 16. In addition, the crest-trough asymmetry appears also slightly enhanced when increasing the amplitude ratio, even after the demodulation of the extreme wave.

All nonlinear effects are consequently considered in the TR procedure (including e.g. the second and third-order ones at play in the previous physical features). This is of primary importance for the accuracy of the reconstruction procedure.

3.3. *Experimental step 2: Refocusing of extreme waves using TR*

TR procedure is applied to the recorded temporal free surface profile, obtained from the mirror position that corresponds to the wave gauge location. This time-reversed signal is then generated by the wave maker. Note that for each wave profile four different amplitude ratios are tested first to describe the effect of nonlinearities while three different probes are used to evaluate the effects of dispersion. We refer to table 6 for the observations during the different experiments.

To assess the accuracy of the reproduction, two estimators are introduced. These are the error on the crest amplitude ϵ_c and the global error on the free surface elevation ϵ_η corresponding to the normalized mean square error of the reproduction procedure. They are defined as:

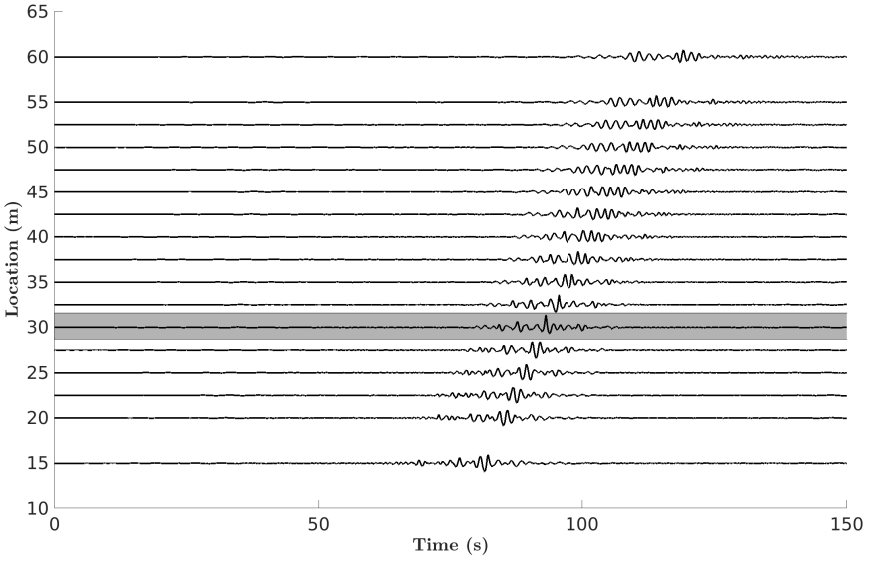

FIGURE 6. Refocusing of the extreme event on probe No. 6 (identified in grey). New Year wave, 100% amplitude. Probes signals are vertically shifted with respect to their location in the wave tank.

$$\epsilon_c = 1 - \frac{\max_t(\eta_{TR}(t))}{\max_t(\eta_t(t))} \tag{3.1}$$

$$\epsilon_\eta = \frac{\int_0^{T_{win}} |\eta_{TR}(t) - \eta_t(t)|^2 \, dt}{\int_0^{T_{win}} |\eta_t(t)|^2 \, dt}, \tag{3.2}$$

with $\eta_t(t)$ being the temporal target free surface profile (*i.e.* the signal recorded at sea) and $\eta_{TR}(t)$ the temporal free surface profile obtained after TR. Note that values close to zero for both errors correspond to an efficient reproduction procedure.

3.3.1. *New Year wave*

An example of wave refocusing is presented in figure 6, making use of the whole set of available wave gauges, in order to observe the unidirectional space-time evolution in the wave tank. The different probes records are vertically shifted with respect to their location in the water tank.

The reproduction location of the extreme wave is the probe No. 6, which is identified in the grey zone in the plot. The refocusing process is indeed clearly observed and confirmed, followed by the demodulation of the extreme event created exactly at the target location x_M.

Figure 7 presents the space-time evolution of the envelope of the signal, which is a typical representation in the context of NLSE. The time has been adjusted by the value

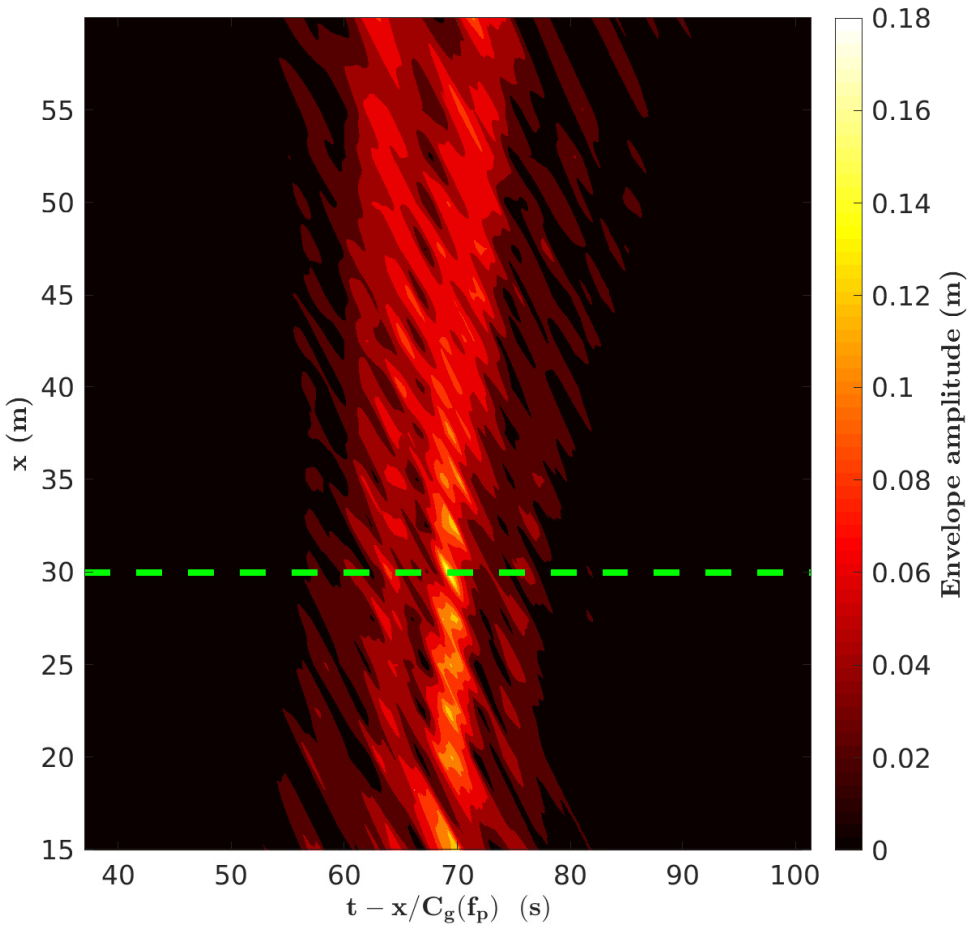

FIGURE 7. Refocusing of the extreme event, space-time representation. New Year wave, 100% amplitude, refocusing on probe No. 6 (identified with the green dashed line)

of the group velocity at the peak of the spectrum $C_g(f_p)$ in order to align the propagation of wave packets only.

The focusing/defocusing process is also quite clear with a change in the amplitude of the envelope together with an increase of its spatial spreading after the reproduction of the rogue event in the wave flume.

In order to quantify the analysis, the reproduced wave profiles need to be compared with the target wave signal and evaluate the error estimators previously introduced. These are ϵ_c and ϵ_η. As an example of results, figure 8 depicts the comparison of the temporal free surface profiles of the reproduction of the New Year wave on the probe No. 1 for the different amplitude ratios [30; 60; 85; 100]%.

The effect of nonlinearity in the TR reconstruction process TR appears to be obvious. While with an amplitude ratio of 30%, the wave profile is perfectly reproduced over the whole time window, discrepancies are more important with an increase of the amplitude

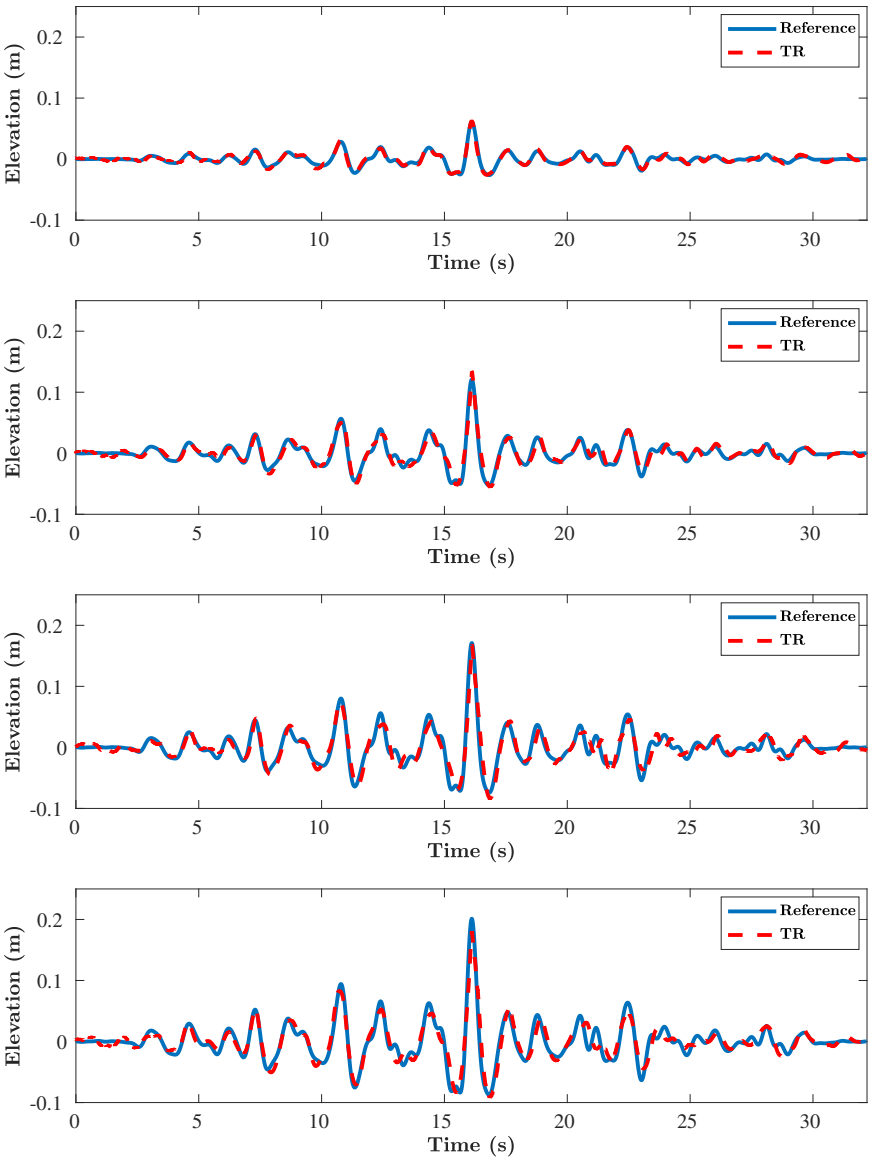

FIGURE 8. Comparison of the original wave profile and the TR reconstructions at probe No. 1 $x_M = 15$ m. New Year wave with different amplitude ratios, [30; 60; 85; 100]% from top to bottom.

and thus, nonlinearity. This confirms previous study results reported in (Ducrozet *et al.* 2016*b*). However, the error remains remarkably limited in the present configuration for all amplitudes.

As indicated in table 6, the first propagation at 100% amplitude is subjected to a local wave breaking close to the wave maker. It is striking that even in the presence of this irreversible process, the TR procedure is accurate in reproducing the initial wave profile ($\epsilon_\eta = 0.09$), with a minor loss of the amplitude of the crest ($\epsilon_c = 0.10$). The breaking process probably removes a limited amount of energy, allowing an accurate reproduction

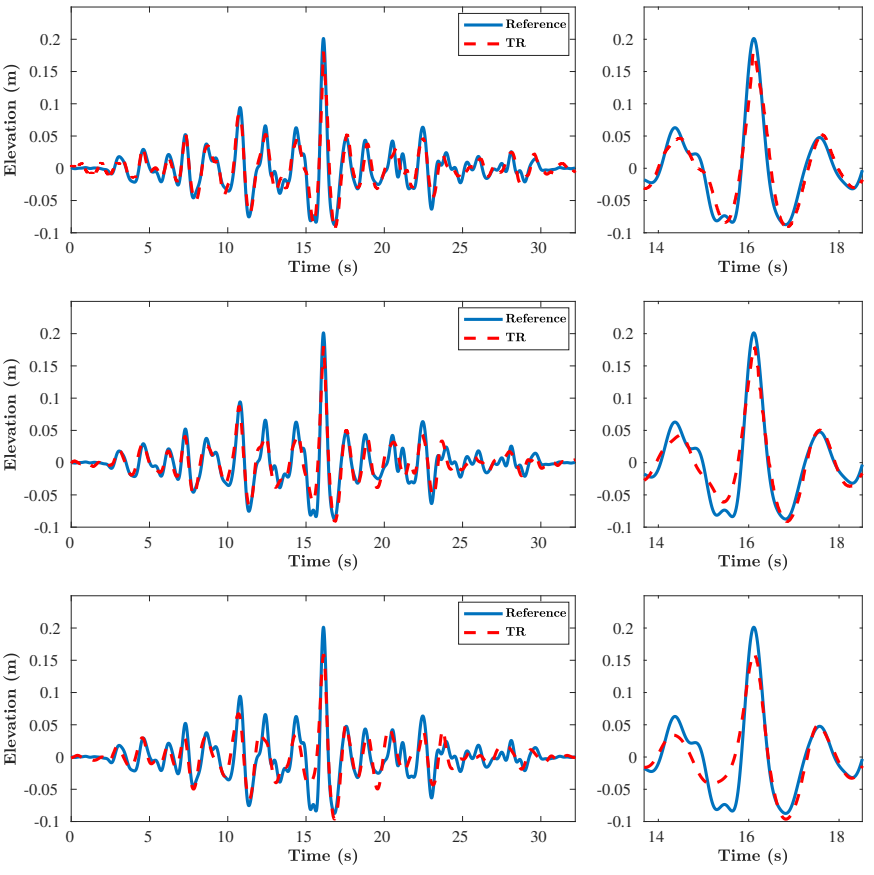

FIGURE 9. Comparison between original wave temporal profile and after TR for New Year wave at 100% amplitude scale. Different mirror locations, probes No. $\in [1;\ 6;\ 16]$ from top to bottom. Complete reconstructed wave profile (left) and zoom on the extreme event (right).

of the target wave profile.

In order to characterize the dispersive effects over the propagating distance, figure 9 depicts the reproduced free surface profiles at the three different locations corresponding to probes No. 1, 6 and 16 for the case of the New Year wave at 100% amplitude scale. As a reminder, the corresponding propagating distances are $[4\lambda_p;\ 8\lambda_p;\ 15\lambda_p]$ respectively.

In addition to the temporal free surface profiles, figure 10 shows the magnitude of the Fourier components of the signal $Y(f)$. This allows a more accurate characterization of the differences between the target signal and the reproduced one.

It is evident that the TR procedure is highly influenced by the propagating distance, thus, dispersive effects, which deteriorate the quality of the reproduction. The comparisons in the time and frequency domains demonstrate significant differences between the target and reproduced signals, especially at the probe No. 16 location. As noted in Sec. 3.2, this last probe is expected to be influenced by the waves reflected from the absorbing beach. This observation holds true for the first propagation as well as for the refocusing experiment.

The analysis of the frequency domain comparison indicates that the discrepancies between target and reproduced signals become increasingly important in the lower

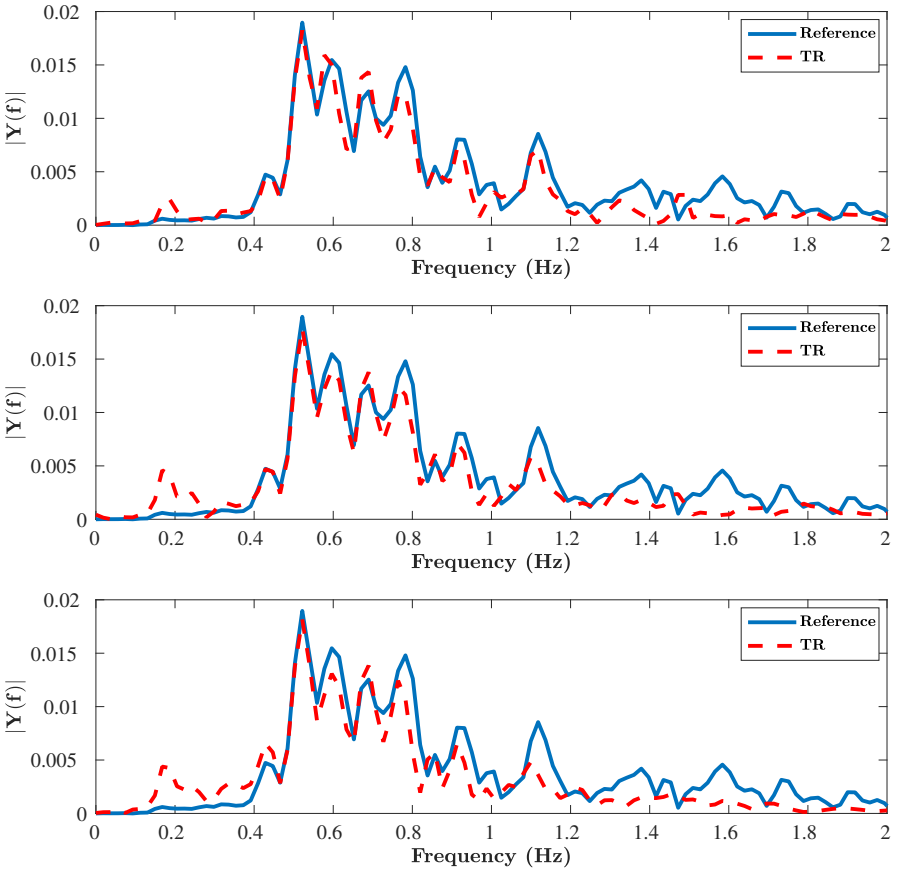

FIGURE 10. Comparison between Fourier Transforms modulus of the original wave profile and after TR for New Year wave at 100% amplitude scale. Different mirror locations, probes No. $\in [1;\ 6;\ 16]$ from top to bottom.

part of the spectrum when increasing the propagating distance. This is indeed a direct consequence of the wave reflection that concerns primarily the fastest wave components.

Some discrepancies are also observed in the high frequency range of the spectrum $f > f_p$, that may be attributed to the residual inaccuracies in the wave generation, even with the second-order corrections provided in the present study. Those may be enhanced during the propagation process due to the different nonlinear interactions between components.

In order to quantify these observations, figure 11 gives the errors on the amplitude of the crest as well as the one on the whole temporal profile for the New Year wave. It allows analysing the accuracy of the method of reproduction, similarly to the numerical work of (Ducrozet *et al.* 2016*b*). The location of the mirror and the amplitude ratio are varied, to assess the effects of dispersion and nonlinearity respectively.

We recover the influences previously described, namely, that an increased propagating distance reduces the accuracy of the reproduction. At the same time, an increased nonlinearity is also affecting the TR procedure, however, in a more limited way. The level of accuracy are indeed satisfying in the range $k_p x_M \leqslant 50$.

The TR procedure, which is a straightforward process to set-up experimentally com-

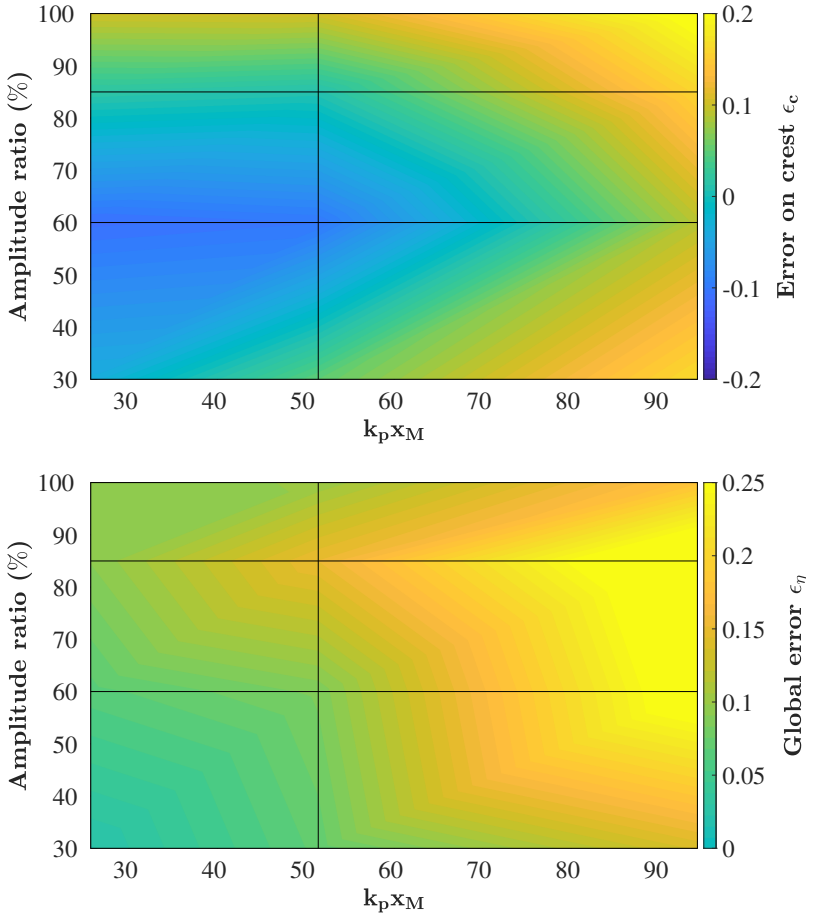

FIGURE 11. Quality of TR reconstruction for the New Year wave as a function of mirror location and amplitude ratio. (Top) Error on crest amplitude ϵ_c. (Bottom) Global error on free surface elevation ϵ_η.

pared to existing ones based on dispersive focusing, such as the New Wave Theory, (Tromans *et al.* 1991; Chaplin 1996; Clauss & Schmittner 2007; Schmittner *et al.* 2009; Fernandez *et al.* 2014; Ducrozet *et al.* 2016*a*), consequently, manages to accurately reproduce highly nonlinear extreme events such as the New Year wave in a straightforward way. The presence of wave breaking during the first experiment or during the refocusing did not lead to a failure of the complete procedure, demonstrating its robustness.

3.3.2. *Yura 1 wave*

Figure 12 presents the overview of the errors after reproduction with a varying level of nonlinearity and propagating distance in the case of the Yura 1 wave field. As a reminder, this rogue wave, compared to the previous New Year wave, appeared in a wave field with lower steepness, but exhibited a larger abnormality index $H_{\max}/H_s$ that corresponds to a lower probability of occurrence (see table 1).

The results for the Yura 1 wave appear similar to the one obtained for the New Year wave. Indeed, an increased steepness of the wave profile to reproduce an increased relative propagating distance induce a reduction of the accuracy of the reproduction,

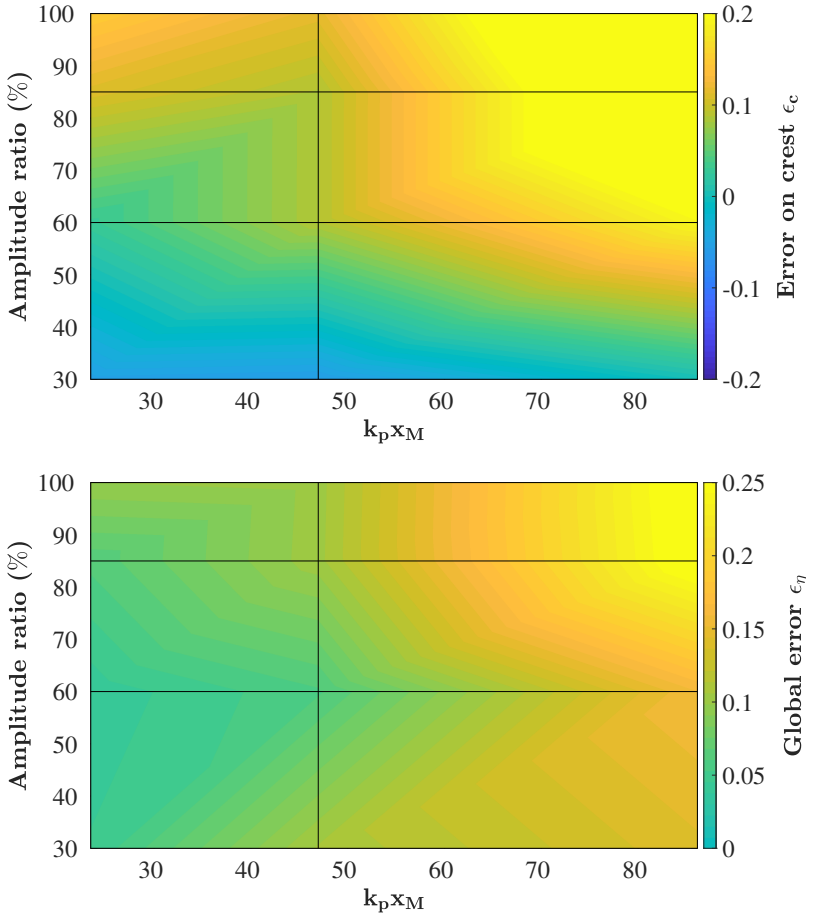

FIGURE 12. Quality of TR reconstruction for the Yura 1 wave as a function of mirror location and amplitude ratio. (Top) Error on crest amplitude ϵ_c. (Bottom) Global error on free surface elevation ϵ_η.

both in terms of the maximum amplitude of the reproduced wave ϵ_c and global error ϵ_η.

We also observe that the free surface profile of the 100% amplitude on probe No. 1 appears less accurate for this wave profile. As a matter of completeness figures 9 & 10, figure 13 presents the comparison of the target and reproduced wave profiles for this specific configuration.

As noted in table 6, wave breaking has been observed during the refocusing experiment for this specific configuration. It takes place at the exact location of the probe, as a result of the high degree of nonlinearity of this wave. For the New Year wave, it was clear that the breaking occurs after the target wave probe when using probe No. 1. This is different for the present configuration in which the breaking appears close and just prior to the probe and is consequently expected to dissipate a part of the wave energy. This induces different behaviours in both configurations and especially for the Yura 1 wave a less accurate reconstruction on probe No. 1, which exhibits an error of $\epsilon_c = 0.15$ and $\epsilon_\eta = 0.10$, respectively.

Nevertheless, the level of errors are notably good for the Yura 1 wave profile over

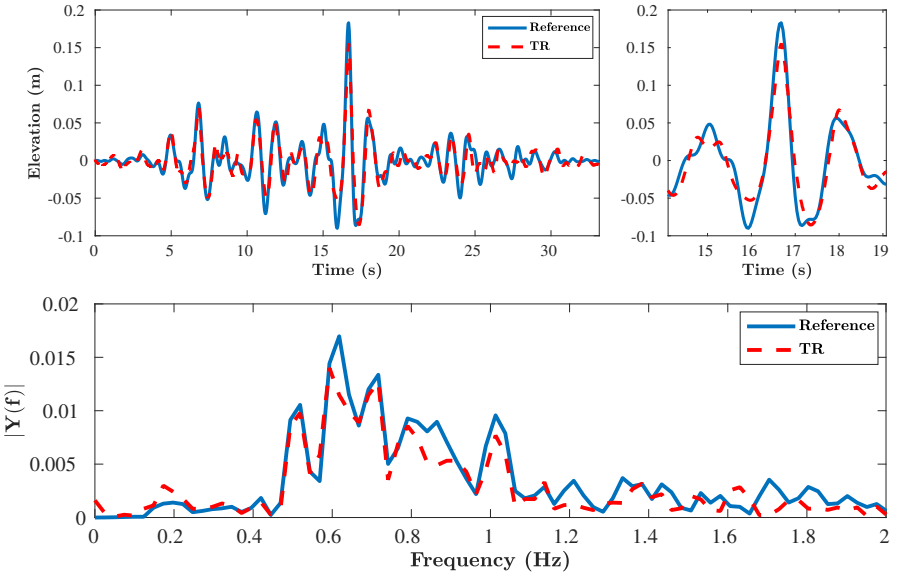

FIGURE 13. Comparison between original wave profile and after TR construction for Yura 1 wave at 100% amplitude scale at probe No 1. (Top) Time domain. (Bottom) Frequency domain.

the whole range of amplitudes up to the most extreme measured one and for limited propagating distances $kx_M \leqslant 50$.

3.3.3. *Yura 2 wave*

The Yura 2 wave has the lowest abnormality index value among the three tested, see main characteristics in table 1. Figure 14 shows the overview of the errors after reproduction with a varying level of nonlinearity and dispersive length.

The observations are similar to the previous ones. These are mainly the increase of the propagating distance and degree of nonlinearity reduces the accuracy of the reconstruction using TR procedure. However, when comparing the results to the features of the New Year and Yura 1 waves as depicted in figures 11 & 12, we annotate that the errors are far smaller for Yura 2 wave profile. This is a direct consequence of the reduced degree of nonlinearity of this wave profile, which is less steep compared to the previous wave configurations. To quantify those differences and as a matter of comparison, figure 15 present the target and reproduced free surface profile for the 100% amplitude scale at the location of probe No. 1.

As expected, the reproduction appears very accurate in this configuration. It is characterized by errors $\epsilon_c = 0.06$ and $\epsilon_\eta = 0.07$. The remaining differences may be attributed to the reflections and other discrepancies that may appear in the course of the TR procedure and during the wave generation.

4. Conclusion

The present work reports a detailed study on the use of the TR methodology for the reproduction of recorded real-world extreme waves in physical unidirectional wave tanks. The objective is to assess the applicability and accuracy of the TR reproduction procedure in this new configuration consisting of genuine rogue waves, embedded in their

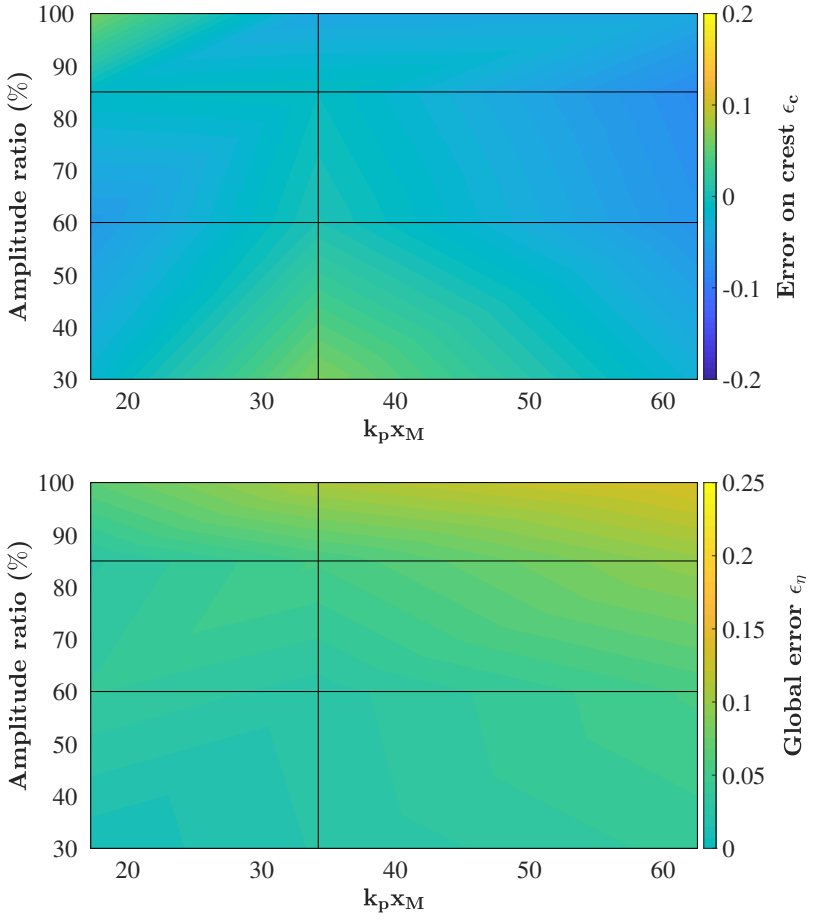

FIGURE 14. Quality of TR reconstruction for the Yura 2 wave as a function of mirror location and amplitude ratio. (Top) Error on crest amplitude ϵ_c. (Bottom) Global error on free surface elevation ϵ_η.

irregular sea-state. To this end, a set of experiments has been carried out in the 140 m long towing tank of ECN. Different wave profiles, obtained from real measurements at sea, have been used: i) the famed New Year wave and ii) two freak wave events recorded in the Sea of Japan.

The design of model-scale experiments for ocean waves is done using Froude scaling. However, it is applied here in a wave tank of arbitrary water depth, due to experimental constraints. The relative water depth is consequently different in model-scale and full-scale configurations, leading in possible different physical processes during wave propagation. Nevertheless, the different features of the TR practice revealed in the current experiments are expected to be relevant when exact Froude scaling is used.

The experiments have been designed to possibly test the influence of the two main parameters exhibited in (Ducrozet *et al.* 2016*b*), namely, the relative propagation distance $k_p x_M$ or dispersive length and the effect of the degree of nonlinearity, independently of the generation mechanism at play. These parameters have been varied over a wide range and have been demonstrated to be also of major importance in the present configuration and study.

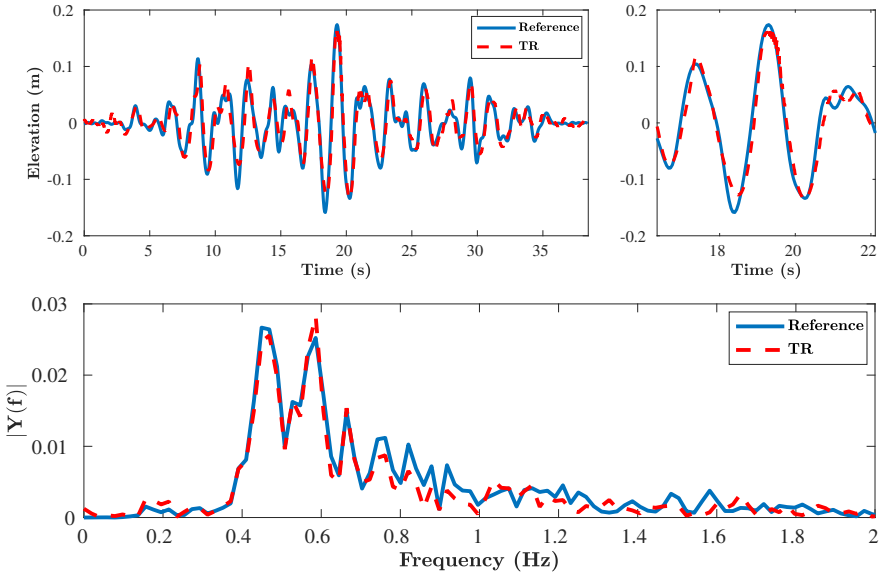

FIGURE 15. Comparison between original wave profile and TR reconstruction for the Yura 2 wave at 100% amplitude scale at probe No. 1. (Top) Time domain. (Bottom) Frequency domain.

We confirmed that the experimental two-step TR procedure can indeed be used for the reproduction of realistic ocean extreme waves in a laboratory environment. The main advantage of the methodology is the refocusing generation of extreme waves at almost any arbitrary position in the wave facility independently of the focusing mechanism at play. An increased steepness of the targeted wave profile and an increase of the relative propagating distance influence the accuracy of the reproduction. The levels of errors observed experimentally with a real free surface measurement of a rogue wave appear similar to the one observed experimentally (Chabchoub & Fink 2014) and numerically validated (Ducrozet *et al.* 2016*b*) using analytic solutions of the NLSE, such as the doubly-localised Peregrine-type breathers (Chabchoub *et al.* 2016) known to be considered as possible backbone prototype rogue waves (Shrira & Geogjaev 2010; Akhmediev *et al.* 2009).

The only discrepancies observed are relative to the spatial extent, which is rather limited in the present experiments compared to the numerical computations. The influence of the relative propagating distance appeared to be driven by the presence of wave reflection instead of presenting a possible inherent limitation of the methodology. Further work using a Numerical Wave Tank that includes all physical processes at play, such as HOS-NWT (Ducrozet *et al.* 2012) may be useful in this context as well. This would allow overcoming the physical limitations of experimental wave flume configurations in terms of dimensions, presence of wave reflections and limited frequency range. These limitations can be mastered in numerical wave tank experiments.

We demonstrated that the TR method is suitable to accurately reconstruct the free surface profile of different rogue wave measurements. In the context of wave-structure interactions, the induced kinematics are also of major importance. These are known to be complex and highly influenced by the wave nonlinearities for extreme waves (Yasuda *et al.* 1994; Grue & Jensen 2006; Alberello *et al.* 2018). However, it is expected that once the free surface profile is accurately reproduced, the induced kinematics naturally follow

(Ducrozet *et al.* 2016*a*). This particular point will be the subject of further investigations.

In addition to the evidence of its accuracy in the current context, the behaviour of the TR procedure in terms of robustness is outstanding. We demonstrated that the presence of marginal wave breaking during the first propagation or during the refocusing did not lead to a failure of the complete refocusing process. Indeed, general physical limitations when reconstructing rogue waves in the wave flume may be attributed to the presence of wave breaking and the presence of wave reflection.

Despite the slight inaccuracies, the TR principle seems to be the simplest procedure to reconstruct highly nonlinear and steep waves in a wave flume compared to existing procedures (Tromans *et al.* 1991; Chaplin 1996; Clauss & Schmittner 2007; Schmittner *et al.* 2009; Fernandez *et al.* 2014; Ducrozet *et al.* 2016*a*), since it provides a similar level of accuracy and high robustness, independently of the physical complexities that were at play in the ocean environment.

Acknowledgments

The authors are grateful to Dr. Sverre Haver for providing the experimental data of the New Year wave. Dr. Sylvain Bourdier is acknowledged for the help provided during the course of the experiments.

Declaration of Interests

None

REFERENCES

Akhmediev, Nail, Ankiewicz, Adrian & Taki, Majid 2009 Waves that appear from nowhere and disappear without a trace. *Physics Letters A* **373** (6), 675–678.

Akhmediev, N, Eleonskii, VM & Kulagin, NE 1985 Generation of periodic trains of picosecond pulses in an optical fiber: exact solutions. *Sov. Phys. JETP* **62** (5), 894–899.

Alberello, Alberto, Chabchoub, Amin, Monty, Jason P, Nelli, Filippo, Lee, Jung Hoon, Elsnab, John & Toffoli, Alessandro 2018 An experimental comparison of velocities underneath focussed breaking waves. *Ocean Engineering* **155**, 201–210.

Babanin, Alexander 2011 *Breaking and dissipation of ocean surface waves*. Cambridge University Press.

Baldock, TE, Swan, C & Taylor, PH 1996 A laboratory study of nonlinear surface waves on water. *Philosophical Transactions of the Royal Society of London. Series A: Mathematical, Physical and Engineering Sciences* **354** (1707), 649–676.

Carminati, R, Pierrat, R, De Rosny, J & Fink, M 2007 Theory of the time reversal cavity for electromagnetic fields. *Optics letters* **32** (21), 3107–3109.

Chabchoub, A. & Fink, M. 2014 Time-reversal generation of rogue waves. *Phys. Rev. Lett.* **112** (124101).

Chabchoub, Amin, Onorato, Miguel & Akhmediev, Nail 2016 Hydrodynamic envelope solitons and breathers. In *Rogue and Shock Waves in Nonlinear Dispersive Media*, pp. 55–87. Springer.

Chaplin, J.R. 1996 On frequency-focusing unidirectional waves. *Int. J. Offshore and Polar Engng.* **6** (2), 131–137.

Clauss, GF & Klein, M 2011 The new year wave in a seakeeping basin: Generation, propagation, kinematics and dynamics. *Ocean Engineering* **38** (14-15), 1624–1639.

Clauss, G. & Schmittner, C. 2007 Experimental optimization of extreme wave sequences for the deterministic analysis of wave/structure interaction. *J. Offshore Mech. and Arctic Engng.* **129**, 61–67.

Cousins, Will & Sapsis, Themistoklis P 2016 Reduced-order precursors of rare events in unidirectional nonlinear water waves. *Journal of Fluid Mechanics* **790**, 368–388.

Dalzell, J.F. 1999 A note on finite depth second-order wave-wave interactions. *Applied Ocean Research* **21** (3), 105 – 111.

Dean, Robert G & Dalrymple, Robert A 1991 *Water wave mechanics for engineers and scientists*, , vol. 2. World Scientific Publishing Company.

Ducrozet, Guillaume, Bonnefoy, Félicien & Ferrant, Pierre 2016*a* On the equivalence of unidirectional rogue waves detected in periodic simulations and reproduced in numerical wave tanks. *Ocean Engineering* **117**, 346–358.

Ducrozet, Guillaume, Bonnefoy, Félicien, Le Touzé, David & Ferrant, Pierre 2012 A modified high-order spectral method for wavemaker modeling in a numerical wave tank. *European Journal of Mechanics - B/Fluids* **34**, 19 – 34.

Ducrozet, Guillaume, Bonnefoy, Félicien & Perignon, Yves 2017 Applicability and limitations of highly non-linear potential flow solvers in the context of water waves. *Ocean Engineering* **142**, 233–244.

Ducrozet, G., Fink, M. & Chabchoub, A. 2016*b* Time-reversal of nonlinear waves: Applicability and limitations. *Phys. Rev. Fluids* .

Dudley, John M, Dias, Frédéric, Erkintalo, Miro & Genty, Goëry 2014 Instabilities, breathers and rogue waves in optics. *Nature Photonics* **8** (10), 755.

Fedele, Francesco, Brennan, Joseph, De León, Sonia Ponce, Dudley, John & Dias, Frédéric 2016 Real world ocean rogue waves explained without the modulational instability. *Scientific reports* **6**, 27715.

Fernandez, H., Sriram, V., Schimmels, S. & Oumeraci, H. 2014 Extreme wave generation using self correcting method ? revisited. *Coastal Engineering* **93** (0), 15 – 31.

Fink, Mathias 1992 Time reversal of ultrasonic fields. i. basic principles. *IEEE transactions on ultrasonics, ferroelectrics, and frequency control* **39** (5), 555–566.

Fink, Mathias 1999 Time-reversed acoustics. *Scientific American* **281** (5), 91–97.

Fouque, Jean-Pierre & Nachbin, André 2003 Time-reversed refocusing of surface water waves. *Multiscale Modeling & Simulation* **1** (4), 609–629.

Fujimoto, Wataru, Waseda, Takuji & Webb, Adrean 2019 Impact of the four-wave quasi-resonance on freak wave shapes in the ocean. *Ocean Dynamics* **69** (1), 101–121.

Grue, John & Jensen, Atle 2006 Experimental velocities and accelerations in very steep wave events in deep water. *European Journal of Mechanics-B/Fluids* **25** (5), 554–564.

Haver, S. 2004 A possible freak wave event measured at the Draupner Jacket January 1 1995. In *Proc. of Rogue Waves 2004*. Brest, France, available at: http://www.ifremer.fr/web-com/stw2004/rw/.

Haver, S., Eik, K.J. & Meling, T.S. 2002 On the prediction of wave crest height extremes. *Tech. Rep.*. Statoil.

Kharif, C, Pelinovsky, E & Slunyaev, A 2009 Rogue waves in the ocean, observation, theories and modeling. In *Advances in geophysical and environmental mechanics and mathematics series*, , vol. 14. Springer Berlin.

Liu, Paul C & Mori, Nobuhito 2001 Characterizing freak waves with wavelet transform analysis. In *Proceedings of Rogue Waves 2000 Workshop*, pp. 151–156.

McAllister, ML, Draycott, S, Adcock, TAA, Taylor, PH & Van Den Bremer, TS 2019 Laboratory recreation of the draupner wave and the role of breaking in crossing seas. *Journal of Fluid Mechanics* **860**, 767–786.

Mori, N., Onorato, M. & Janssen, P.A.E.M. 2011 On the estimation of kurtosis in directional sea states for freak waves forecasting. *J. Phys. Ocean.* **41**, 1484–1496.

Onorato, Miguel, Residori, S, Bortolozzo, U, Montina, A & Arecchi, FT 2013 Rogue waves and their generating mechanisms in different physical contexts. *Physics Reports* **528** (2), 47–89.

Onorato, Miguel, Waseda, T, Toffoli, A, Cavaleri, L, Gramstad, O, Janssen, PAEM, Kinoshita, T, Monbaliu, Jaak, Mori, N, Osborne, Alfred Richard & others 2009 Statistical properties of directional ocean waves: the role of the modulational instability in the formation of extreme events. *Physical review letters* **102** (11), 114502.

Peregrine, DH 1983 Water waves, nonlinear schrödinger equations and their solutions. *The ANZIAM Journal* **25** (1), 16–43.

Przadka, A., Feat, S., Petitjeans, P., Pagneux, V., Maurel, A. & Fink, M. 2012 Time reversal of water waves. *Phys. Rev. Lett.* **109**, 064501.

Schäffer, H.A. 1996 Second-order wavemaker theory for irregular waves. *Ocean Engng.* **23** (1), 47–88.

Schmittner, C., Kosleck, S. & Hennig, J. 2009 A phase-amplitude iteration scheme for the optimization of deterministic wave sequences. In *Proc of the* 28^{th} *Int. Conf. Ocean, Offshore and Arctic Engng.*. Honolulu, Hawaii, USA.

Shemer, L, Goulitski, K & Kit, E 2007 Evolution of wide-spectrum unidirectional wave groups in a tank: an experimental and numerical study. *European Journal of Mechanics-B/Fluids* **26** (2), 193–219.

Shrira, Victor I & Geogjaev, Vladimir V 2010 What makes the peregrine soliton so special as a prototype of freak waves? *Journal of Engineering Mathematics* **67** (1-2), 11–22.

Tromans, Peter S, Anaturk, Ali R, Hagemeijer, Paul & others 1991 A new model for the kinematics of large ocean waves-application as a design wave. In *The First International Offshore and Polar Engineering Conference*. International Society of Offshore and Polar Engineers.

Yasuda, T, Mori, N, Nakayama, S & others 1994 Freak wave kinematics in unidirectional deep water waves. In *The Fourth International Offshore and Polar Engineering Conference*. International Society of Offshore and Polar Engineers.

Zakharov, Vladimir E 1968 Stability of periodic waves of finite amplitude on the surface of a deep fluid. *Journal of Applied Mechanics and Technical Physics* **9** (2), 190–194.